Micromanipulation of InP lasers with optoelectronic tweezers for integration on a photonic platform

JOAN JUVERT,[1,*] SHUAILONG ZHANG,[1] IAIN EDDIE,[2] COLIN J. MITCHELL,[3] GRAHAM T. REED,[3] JAMES S. WILKINSON,[3] ANTHONY KELLY,[1] AND STEVEN NEALE[1]

[1] School of Engineering, University of Glasgow, 79 Oakfield Ave., Glasgow, United Kingdom
[2] CST Global Ltd., 4 Stanley Boulevard, Hamilton, United Kingdom
[3] Optoelectronics Research Centre, University of Southampton, Southampton, Hampshire, SO17 1BJ, United Kingdom
*joan.juvert@glasgow.ac.uk

Abstract: The integration of light sources on a photonic platform is a key aspect of the fabrication of self-contained photonic circuits with a small footprint that does not have a definitive solution yet. Several approaches are being actively researched for this purpose. In this work we propose optoelectronic tweezers for the manipulation and integration of light sources on a photonic platform and report the positional and angular accuracy of the micromanipulation of standard Fabry-Pérot InP semiconductor laser die. These lasers are over three orders of magnitude bigger in volume than any previously assembled with optofluidic techniques and the fact that they are industry standard lasers makes them significantly more useful than previously assembled microdisk lasers. We measure the accuracy to be 2.5 ± 1.4 μm and 1.4 ± 0.4 ° and conclude that optoelectronic tweezers are a promising technique for the micromanipulation and integration of optoelectronic components in general and semiconductor lasers in particular.

OCIS codes: (250.5960) Semiconductor lasers; (230.2090) Electro-optical devices; (350.4855) Optical tweezers or optical manipulation.

References and links

1. H. Kawanami, "Heteroepitaxial technologies of III-V on Si," Sol. Energ. Mat. Sol. C. **66**, 479–486 (2001).
2. D. Pasquariello and K. Hjort, "Plasma-assisted InP-to-Si low temperature wafer bonding," IEEE J. Sel. Top. Quant. **8**, 118–131 (2002).
3. G. Roelkens, L. Liu, D. Liang, R. Jones, A. Fang, B. Koch, and J. Bowers, "III-V/silicon photonics for on-chip and intra-chip optical interconnects," Laser Photonics Rev. **4**, 751–779 (2010).
4. K. Tanabe, D. Guimard, D. Bordel, S. Iwamoto, and Y. Arakawa, "Electrically pumped 1.3 micron room-temperature InAs/GaAs quantum dot lasers on Si substrates by metal-mediated wafer bonding and layer transfer." Opt. Express **18**, 10604–10608 (2010).
5. S. Famenini and C. G. Fonstad, "Integration of edge-emitting laser diodes with dielectric waveguides on silicon," IEEE Photonic Tech. L. **24**, 1849–1851 (2012).
6. K. Samonji, H. Yonezu, Y. Takagi, K. Iwaki, N. Ohshima, J. K. Shin, and K. Pak, "Reduction of threading dislocation density in InP-on-Si heteroepitaxy with strained short-period superlattices," Appl. Phys. Lett. **69**, 100 (1996).
7. M. Yamaguchi, M. Sugo, and Y. Itoh, "Misfit stress dependence of dislocation density reduction in GaAs films on Si substrates grown by strained-layer superlattices," Appl. Phys. Lett. **54**, 2568–2570 (1989).
8. H. Park, M. Sysak, and H. Chen, "Device and integration technology for silicon photonic transmitters," IEEE J. Sel. Top. Quant. **17**, 671–688 (2011).
9. P. Y. Chiou, A. T. Ohta, and M. C. Wu, "Massively parallel manipulation of single cells and microparticles using optical images." Nature **436**, 370–372 (2005).
10. S. L. Neale, Z. Fan, a. T. Ohta, a. Jamshidi, J. K. Valley, H. Y. Hsu, a. Javey, and M. C. Wu, "Optofluidic assembly of red / blue / green semiconductor nanowires," in *Conference on Lasers and Electro-Optics and Quantum Electronics and Laser Science Conference (CLEO/QELS 2009)*.
11. M. C. Tien, A. T. Ohta, K. Yu, L. C. Chuang, A. Jamshidi, S. L. Neale, C. Hou, C. Chang-Hasnain, and M. C. Wu, "Hybrid microdisk laser on a silicon platform using lateral-field optoelectronic tweezers assembly," in *Conference on Lasers and Electro-Optics and Quantum Electronics and Laser Science Conference on Lasers and Electro-Optics (CLEO/QELS 2008)*.

12. H. I. Cantú, A. McKee, I. Eddie, and A. E. Kelly, "Parametric study of 1310 nm ridge waveguide AlGaInAs-InP semi-conductor laser dynamics," IET Optoelectron. **9**, 341–347 (2015).
13. J. K. Valley, A. Jamshidi, A. T. Ohta, H. Y. Hsu, and M. C. Wu, "Operational regimes and physics present in optoelectronic tweezers," J. Microelectromech. S. **17**, 342–350 (2008).
14. H. A. Pohl, *Dielectrophoresis: the Behavior of Neutral Matter in Nonuniform Electric Fields* (Cambridge University, 1978).
15. X. Wang, X.-B. Wang, and P. R. Gascoyne, "General expressions for dielectrophoretic force and electrorotational torque derived using the Maxwell stress tensor method," J. Electrostat. **39**, 277–295 (1997).
16. J. Juvert, I. Eddie, C. Mitchell, G. T. Reed, J. S. Wilkinson, A. Kelly, and S. L. Neale, "A low-cost technique for adding microlasers to a silicon photonic platform," Proc. SPIE 9752, 97520Y (2016).
17. I. Armstrong, I. Andonovic, A. Kelly, S. Bonthron, J. Bebbington, W. Michie, C. Tombling, S. Fasham, and W. Johnstone, "Hybridisation platform assembly and demonstration of all optical wavelength conversion at 10Gbit/s," J. Lightwave Technol. **23**, 1852–1859 (2005).

1. Introduction

Photonic circuits need a light source to drive them, and while it is possible to use a pre-packaged external laser source in some cases, many applications such as on-chip communications require the smaller footprint of an integrated source. Several approaches have been proposed to overcome the lack of an efficient, electrically pumped silicon laser that could be monolithically integrated in a silicon photonics platform. The most promising of these approaches are heteroepitaxial growth of germanium or III-V compounds on silicon [1], wafer bonding [2–4] and active alignment with pick and place tools [5].

Heteroepitaxial growth of germanium or III-V compounds on silicon and wafer bonding have the advantage of high scalability, but they involve trade-offs in terms of performance and reliability of the integrated lasers [6–8]. Furthermore, the integration of light sources with different properties in the same process is challenging with these techniques.

The active alignment approach consists of individually picking complete, pre-fabricated light sources and placing them directly where they need to be, typically with mechanical tools. This is a very flexible approach that allows the integration of different kinds of sources on the same platform, for instance lasers of different wavelengths for wavelength division multiplexing arrangements. Unfortunately, the micromanipulation process is essentially serial, meaning that this approach does not scale well for mass production.

As an alternative to mechanical pick and place tools, we propose optoelectronic tweezers as a tool for the integration of standard InP semiconductor lasers on a photonic platform. Optoelectronic tweezers are based on light-induced dielectrophoresis [9] and have been used successfully in the past for the micromanipulation of semiconductor nanowires [10] and microdisk lasers [11]. Optoelectronic tweezers work with optical power densities as low as $1\,\mathrm{W\,cm^{-2}}$, and the light source used for the creation of the dielectrophoretic traps does not need to be coherent. Therefore, commercial data projectors can be used to pattern the dielectrophoretic traps, which gives the technique great potential for the automation and parallelization of the micromanipulation process [9], making it more suitable for mass integration on a photonic platform.

In this work we study the accuracy of the micromanipulation of standard Fabry-Pérot InP semiconductor die with optoelectronic tweezers. These microlasers are $250\,\mu\mathrm{m}$ across and, to the best of our knowledge, the biggest objects that have been manipulated with optoelectronic tweezers. Furthermore, the fact that they are industry standard makes them more useful than previously reported microdisk lasers [11]. We will simulate the relation between the dielectrophoretic force and the size of the trap in order to find any optimal values, and we will determine experimentally the accuracy of the positioning of the laser die. This is relevant because the accuracy of the positioning of the microlaser die on a photonic platform has a direct impact on the lowest achievable coupling losses to other components of the photonic integrated circuit.
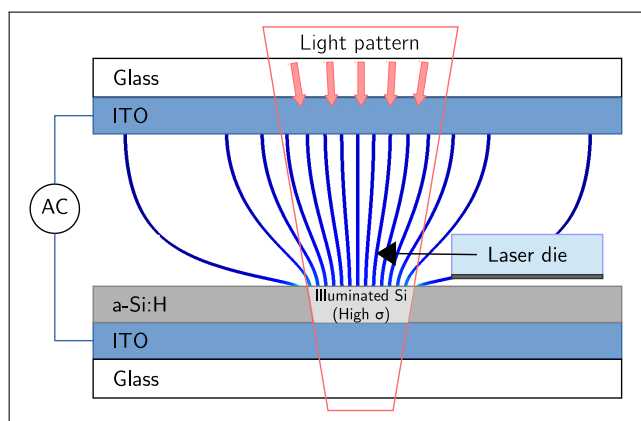
Fig. 1. Schematic representation of the optoelectronic tweezers device. The chamber is realised by inserting a 150 μm thick spacer (double sided tape, not represented) between the top electrode and the the a-Si:H. The blue lines follow the electric field vector.

2. Experimental

Our optoelectronic tweezers device (Fig. 1) consists of two electrodes, both of them a 600 nm thick ITO layer on a glass substrate (Diamond Coatings, UK). The bottom electrode is coated with a 1 μm thick PECVD hydrogenated amorphous silicon layer (a-Si:H) deposited at 300 °C. The two electrodes are vertically stacked with double sided tape between them. The double sided tape acts as a spacer to create a 150 μm thick chamber between the electrodes.

A liquid medium with the laser die in suspension is introduced in the chamber. In our case, the liquid medium is deionised water with added surfactant (Tween 20, SIGMA P9416, one drop per 50 ml of deionized water). The surfactant improves the solubility of the die in the water. The conductivity of the medium is approximately $2 \, \mathrm{mS \, m^{-1}}$. The laser die are placed on the a-Si:H surface with a pipette, between two double sided tape strips, before closing the chamber with the top electrode. The device rests on a motorized stage (Prior H101BX ProScan II).

We bias between the two electrodes with a sinusoidal signal with amplitude 30 V peak to peak at a frequency of 15 kHz from a function generator (TTi TG5011) connected to an amplifier (TTi WA301). 30 V is the maximum voltage allowed by our amplifier, whereas the frequency of 15 kHz has been experimentally found to yield the strongest forces when manipulating the semiconductor laser die of this work.

The dielectrophoretic trap is patterned by focusing the output of a data projector (Dell 1510X) on the a-Si:H layer through a microscope column (Olympus BX51) with a 10x objective. The output of the projector goes through a longpass filter so that the a-Si:H is patterned with red light. The illuminated area of the silicon layer exhibits an enhanced conductivity where the field lines tend to converge, creating the electric field gradient that attracts the semiconductor laser die (see Fig. 1). The chamber is imaged by a camera (Olympus UC30) through a shortpass filter that avoids the saturation of the camera sensor by the bright projected pattern. See Fig. 2 for a schematic representation of the experimental setup.

We can pattern traps of any 2D shape or arbitrary arrangements of multiple traps by sending the appropriate image to the data projector, typically a white pattern on a black background. For our experiments, since the laser die we want to micromanipulate have a square shape, we project square traps of different sizes bigger than the laser die itself. The microlasers experience positive dielectrophoresis and are pulled towards the centre of the trap, where they self-align to match the orientation of the square illumination pattern. Figure 3 shows a laser die trapped
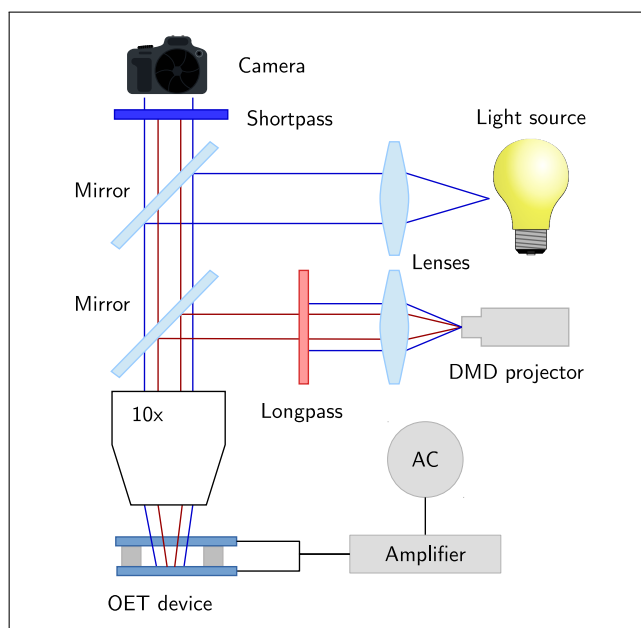
Fig. 2. Schematic representation of the experimental setup used in this work.
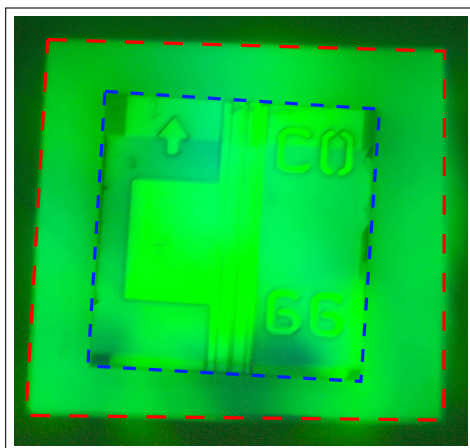

Fig. 3. Picture of a laser die (blue dashed contour) inside a dielectrophoretic trap (red dashed contour). The laser is $250\,\mu m$ on its side. See Visualization 1 for a video showcasing the micromanipulation of the laser die.

inside a light pattern. The light pattern can then be moved around, dragging the laser with it. A video showing a laser die being moved around and rotated can be found in the supplementary materials (Visualization 1)

The die in this work are standard Fabry-Pérot InP semiconductor lasers [12], $250\,\mu m$ across and $100\,\mu m$ thick and have been provided by CST Global Ltd., UK. A detailed description of the structure and properties of the lasers can be found in reference [12].
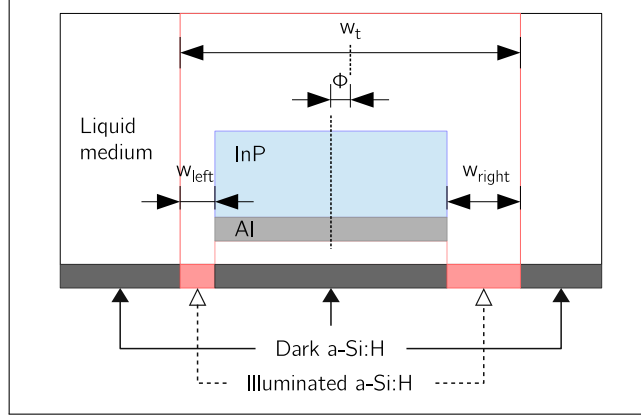
Fig. 4. Schematic representation of the simulated system (not to scale). The relevant parameters are the total width of the trap w_t and the offset ϕ between the centres of the laser and the trap.

3. Simulations

We are interested in the relation between the total dielectrophoretic force on the laser and the size of the trap to see if there is an optimal value. We have simulated the optoelectronic tweezers device of our experiments using the finite elements method (COMSOL Multiphysics). In order to simulate the dielectrophoretic trap, we set the conductivity of the amorphous silicon to $1 \times 10^{-12}\,\mathrm{S\,m^{-1}}$ in the dark regions and $1 \times 10^{-4}\,\mathrm{S\,m^{-1}}$ in the illuminated regions [13]. Since we project the light pattern from the top and the laser blocks some of the light from reaching the photoconductor beneath it, the illuminated area is actually a square band surrounding the laser die. The schematic representation of the simulated 2D system can be found in Fig. 4 (not to scale). The thickness of amorphous silicon layer and the aluminium contact is set to $1\,\mu\mathrm{m}$, and the gap between the laser die and the surface of the amorphous silicon is $1\,\mu\mathrm{m}$ as well. The total thickness of the laser die is $100\,\mu\mathrm{m}$ and the height of the chamber is $150\,\mu\mathrm{m}$.

The voltage at the bottom of the silicon layer is set to 30 V whereas the top of the chamber is set to ground. The lateral edges of the simulation cell are set to electrical insulation and all the inner interfaces to continuity.

The relevant parameters of the simulation are the trap width w_t and the offset ϕ between the centres of the trap and the laser die. Since the width of the laser is $250\,\mu\mathrm{m}$, the total illuminated width is $w_i = w_t - 250\,\mu\mathrm{m}$, of which $w_{\mathrm{left}} = w_i/2 - \phi\,\mu\mathrm{m}$ fall on the left side of the laser and $w_{\mathrm{right}} = w_i/2 + \phi\,\mu\mathrm{m}$ fall on the right side.

We use the simulation to calculate the total dielectrophoretic force on the laser die as a function of the offset ϕ between the trap and the laser for different sizes w_t of the trap. We carry out the calculation using two different formalisms, the effective dipole method and the Maxwell Stress Tensor (MST) method.

3.1. Calculations using the effective dipole moment

The simplest way to calculate the dielectrophoretic force on a spherical particle is with the equation [14]:

$$\vec{F}_{\mathrm{DEP}} = 2\pi r^3 \epsilon_m \mathfrak{R}\left(\frac{\hat{\epsilon}_p - \hat{\epsilon}_m}{\hat{\epsilon}_p - 2\hat{\epsilon}_m}\right)\vec{\nabla}E^2 \,, \tag{1}$$

Here, r is the radius of the particle, ϵ_m is the real part of the electrical permittivity of the medium, $\hat{\epsilon}_p$ and $\hat{\epsilon}_m$ are the complex electrical permittivities of the particle and the medium,

respectively, and E is the external electric field at the center of the particle. The term between parentheses is the real part of the Clausius-Mossotti factor in the case of a spherical particle.

Equation 1 represents the product of the effective dipole moment of the particle (an ideal point dipole located at the centre of the particle that generates the same electric field distribution as the polarized particle) and the gradient of the square of the field.

Unfortunately, our microlaser die is not a spherical particle and therefore we do not know what its Clausius-Mossotti factor is. However, the Clausius-Mossotti factor is a constant scalar value between 1 and −0.5, so it should still be possible to get the correct functional dependence between the force and the offset considering the Clausius-Mossotti factor as 1, even though the numerical values of the force will be off by a constant factor.

Another consideration to make is that the approach that leads to equation 1 assumes small non-uniformities of the field in the volume of the particle. While this will be typically true to a good degree for small dielectric particles that introduce small distortions to the external field, it is not clear that this is the case for metallic beads or our semiconductor laser die, where the distortion of the electric field introduced by the aluminium contact and the n-type bulk InP will be high.

The results of the simulation of the total force on a 2D slice of the microlaser using equation 1 are plotted in Fig. 5 (in $N\,m^{-1}$, since the simulation is 2D). The results are calculated for two sizes of the trap, 250.7 and 270 μm, or 0.7 and 20 μm bigger than the laser, respectively. Note that positive offsets correspond to the trap moving to the right, and from symmetry considerations the results for negative offsets are the same with opposite sign.

The sharp change in the curves of Fig. 5 correspond to the offset where the trap has moved so far to the right that there is no light on the left side of the laser.

The most important feature of these results is that, for wide traps (solid line in Fig. 5), the force is negative for the first few microns of offset. Negative forces mean that the trap pulls the laser to the left. In other words, when the trap moves to the right, the laser tends to move towards the left edge of the trap, and the force does not get positive until the laser is very close to the left edge. This result tells us that the laser is in an unstable equilibrium at the center of the trap, and will tend to fall towards either edge. Once it is at the edge, we do get a restorative force and the laser will follow the trap.

This does not happen for traps barely bigger than the laser. The dashed line in Fig. 5 shows no regions with negative force, which means that the laser moves to the right as soon as we offset the trap to the right (and vice-versa).

From Fig. 5 we can integrate to find the potential energy of the laser die in the trap. The results are shown in Fig. 6 (we have symmetrized the results to give the complete picture). The plots clearly indicate that for big traps there is a potential well at each edge where the laser will tend to align. In order to get a useful restorative force in a single potential well located at the centre of the trap we need to use small traps. To that effect, the simulations indicate that the trap should be smaller than 251.5 μm, that is 1.5 μm bigger than the laser or less.

The results from the simulations that use this approach do not match well with the results found from the physical experiments. Experimentally it is found that the laser die always align with the centre of the trap regardless of the size of the trap, and so another formalism was investigated.

3.2. Calculations using the Maxwell stress tensor

A more exact calculation of the dielectrophoretic force that does not involve the approximations of the previous section, e.g. spherical particle and small non-uniformity of the field gradient, is given by the Maxwell stress tensor [15], which can be derived from the Lorentz force law.
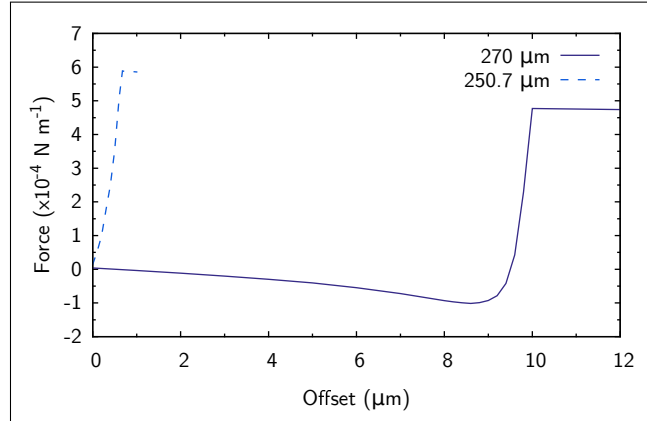
Fig. 5. Total force on the laser as a function of the offset of the trap with respect to the laser, for two different sizes of the trap, calculated using the gradient of the square of the electric field.
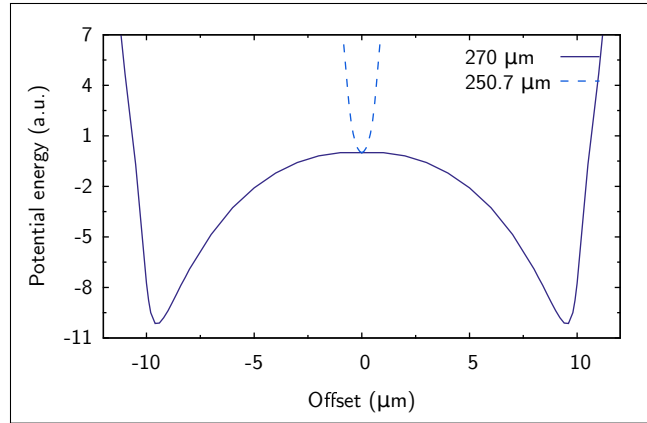

Fig. 6. Potential energy of the laser around the center of dielectrophoretic traps of different sizes. The potential energy has been worked out from the force calculated using the gradient of the square of the electric field (Fig. 5).

$$\sigma_{ij} = \varepsilon_0 E_i E_j + \frac{1}{\mu_0} B_i B_j - \frac{1}{2}\left(\varepsilon_0 E^2 + \frac{1}{\mu_0} B^2\right)\delta_{ij} \qquad (2)$$

Where σ_{ij} is the ij element of the second rank Maxwell stress tensor, ε_0 is the vacuum permittivity, μ_0 is the vacuum permeability, E and B are the electric and magnetic fields, respectively, and δ_{ij} is Kronecker's delta.

The elements σ_{ij} of the Maxwell stress tensor have dimensions of force per unit area in SI units as written in equation 2. In particular, the element ij represents the force per unit area parallel to the i axis suffered by a surface normal to the j axis. The diagonal elements are then pulling forces whereas the off-diagonal elements represent shear stress. Therefore, a 2D integration over the area enclosing a certain volume yields the total force on said volume.

Integration of the Maxwell stress tensor along the boundaries of the laser die gives the results for the force plotted in Fig. 7. Further integration of the results in Fig. 7 gives the potential energy, plotted in Fig. 8.
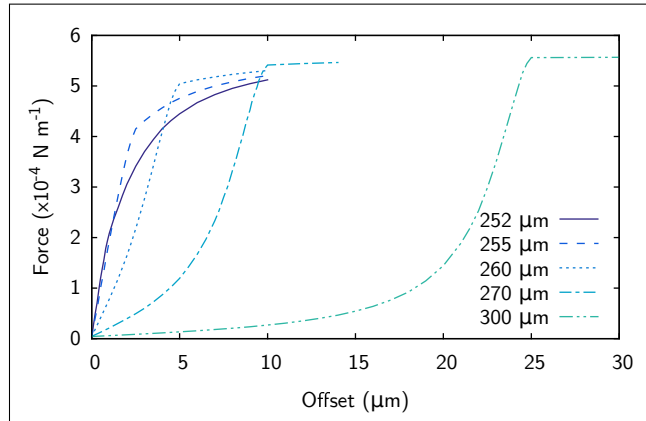
Fig. 7. Total force on the laser as a function of the offset of the trap with respect to the laser, for different sizes of the trap. Calculated using the Maxwell stress tensor.
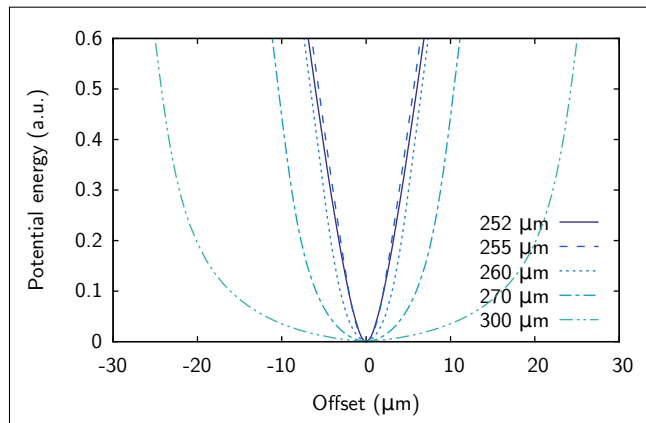

Fig. 8. Potential energy of the laser around the center of dielectrophoretic traps of different sizes. The potential energy has been worked out from the force calculated using the Maxwell stress tensor (Fig. 7).

The results in Figs. 7 and 8 successfully reproduce our experimental observation that the laser die tends to self align to the centre of the trap regardless of its size, since the force always points in the same direction as the offset, e.g. there is always a restoring force towards the centre of the trap.

In addition, from a practical point of view, the results tell us that smaller traps give greater trap stiffness for small displacements from the equilibrium position at the centre of the trap. In the ideal system of our simulations, the size of the trap should not affect the accuracy of the positioning since the restorative force will always bring the laser die to the exact center of the trap. However, in our real experimental setup there are other forces that will limit the accuracy, in particular viscous drag and friction with the surface of the silicon. In this regard, we do expect the size of the trap to affect the accuracy of the positioning, since the dielectrophoretic force will dominate over other forces at smaller offsets when the trap is tighter.

4.   Experimental results

In order to measure the accuracy of the manipulation, we confine a laser in a square dielec-trophoretic trap and move it a few hundred microns to a random position on the device. The microlasers can be moved at speeds in excess of $1\,\text{mm}\,\text{s}^{-1}$, which corresponds to forces in the order of nN (considering the dielectrophoretic force opposes the Stokes' drag). These speeds are high enough that a microlaser can be positioned within a standard $1\,\text{cm}^2$ chip in a few seconds. For the movement of the microlaser, the trap itself is static and we actually move the stage where the device rests, so that the trapped laser moves with respect to the surface of the a-Si:H. After stopping the trap at a random position, we add a random rotation. In the case of the rotation, it is the projected trap itself that rotates. See Visualization 1 in supplementary materials for a video showcasing the manipulation of a microlaser die.

We then take a still of the relative positions of the trap and the laser, such as the one in Fig. 3. We measure the angle between the trap and the laser die using an image processing and analysis software (ImageJ). Using the same software, we find the centres of the trap and the laser die by drawing crosses aligned with the corners of the squares (a cross for the trap and a cross for the laser) and measure the distance between the centres in its x and y components.

The scale of the images corresponds to 3 pixels per micron. Since the edges of the trap and the laser are not absolutely sharp, there is an error involved in the determination of the centres and therefore the offset between them. We estimate the error in the measurement of the distance and the angle to be $\pm1.4\,\mu\text{m}$ and $\pm0.4\,°$, respectively.

For a given microlaser die we repeat this process of random movement and measurement of the offset several times for different trap sizes. Figure 9 shows a scatter plot of the results. Error bars have not been added to the points to aid clarity, but the positions are subject to the aforementioned $1.4\,\mu\text{m}$ measurement error. Each point in the plot corresponds to the position of the same laser with respect to the centre of the trap after moving it to a random position. This particular laser did not move smoothly, probably due to friction with the a-Si:H substrate. As a result, the dispersion of the offsets is quite large and there is no obvious dependence with the size of the trap.

On the other hand, Fig. 10 shows the results for a laser that was more free to move. In this case there is a clear dependence of the dispersion with the size of the trap. While the points corresponding to the biggest trap ($350\,\mu\text{m}$) are scattered across a wide area, the points corresponding to the smallest trap ($260\,\mu\text{m}$) appear nicely clumped together.

Similar differences are observed when we take a look at the angle between the microlaser and the trap (Fig. 11). The "L1" points (dark blue) correspond to the same measurements of Fig. 9, whereas the "L2" points (light blue) correspond to the same measurements of Fig. 10. The observations for the x and y offset apply to the angular offset as well: there is no clear relation between the size of the trap and the dispersion in the angle for the laser that appears to be more affected by friction, whereas for the laser that moves smoothly the dispersion is clearly lower for the smaller trap.

Figures 9 and 10 illustrate our observation that there is a significant difference in the results of different individual die. We have observed that those die that happen to rest on their bottom contact (such as the one illustrated in Fig. 3) generally move smoothly, whereas those that lie on their top sides seem to be more affected by friction. This could be explained by the fact that the bottom contact is a relatively uniform metal layer, whereas the top side has ridges and trenches [12] that make it easier for the laser die to get stuck on the surface of the a-Si:H.

Bearing in mind the simulations in Fig. 7, in the face of strong friction (static or dynamic), not even the relatively strong dielectrophoretic forces near the edge of the trap are strong enough to overcome friction, and therefore the microlaser can get stuck essentially anywhere regardless of the size of the trap. On the other hand, for die that experience lower friction, the relatively weak forces near the centre of big traps could be insufficient to overcome even that small friction
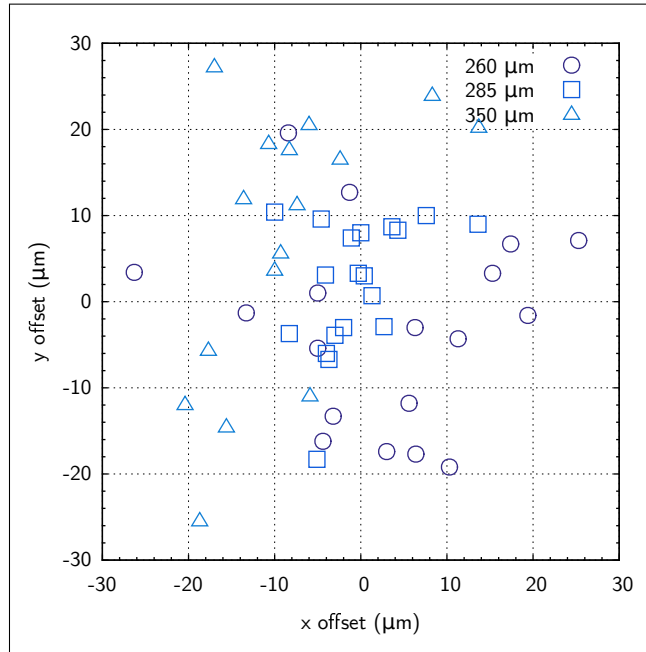
Fig. 9. Offset of the centre of a laser die with respect to the centre of the trap for different sizes of the trap. This laser was face down and did not move smoothly.

threshold and bring the laser close to the centre, whereas smaller traps that exhibit relatively strong forces for small deviations from the centre would be more likely to successfully overcome friction and bring the laser closer to the centre.

Another interesting observation is that in Fig. 10 all the points are in the lower-left half of the area (below the diagonal), and in the case of the points corresponding to the smallest trap they are nicely clumped together not around the centre but with a clear overall offset with respect to the centre of the trap, around $6\,\mu$m from the centre. This can be explained by a combination of effects. Most importantly, the projection of our square trap is neither perfectly square nor perfectly uniform in its illumination intensity. This can be observed in Fig. 3. Nonuniformities in the polarizability of the microlaser could also contribute to this systematic misalignment. Improvement of the projected image with a light field of more uniform intensity and fewer optical aberrations would help reduce this misalignment. However, even if present, the systematic misalignment can easily be accounted for and compensated. For the purpose of estimating the accuracy of the positioning we are more interested in the dispersion of the measurements.

The mean position of the best set of measurements (circles in Fig. 10 is $(-3.8, -5.2)\,\mu$m with a standard deviation of 1.2 and $1.7\,\mu$m for x and y, respectively. However, a better estimate of the accuracy in this case is given by half the difference between the maximum and minimum values, 1.9 and $2.5\,\mu$m for x and y, respectively. The small difference between the values for x and y could be explained by the same reasons as the systematic misalignment with respect to the nominal centre of the trap.

In order to combine the results of x and y in a single figure of merit, we can do the statistical analysis using the absolute distance between the centres of die and trap. In that case we get a mean distance of $6.6\,\mu$m, with a standard deviation of $1.6\,\mu$m and a half difference between minimum and maximum of $2.5\,\mu$m.

As for the angle, the mean value is $-0.6°$ with a standard deviation of $1.0°$ and a half difference of $1.4°$ between maximum and minimum values. As already stated, the error in the
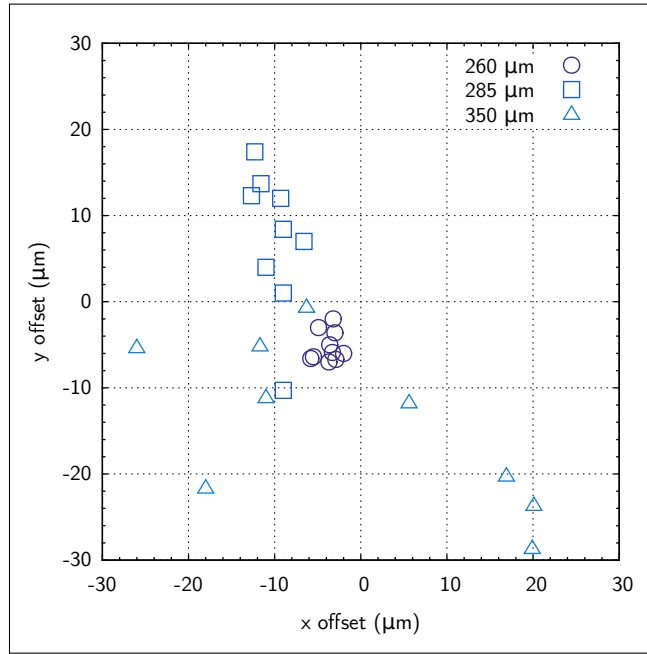
Fig. 10. Offset of the centre of a laser die with respect to the centre of the trap for different sizes of the trap. This laser was face up and showed a smooth movement.
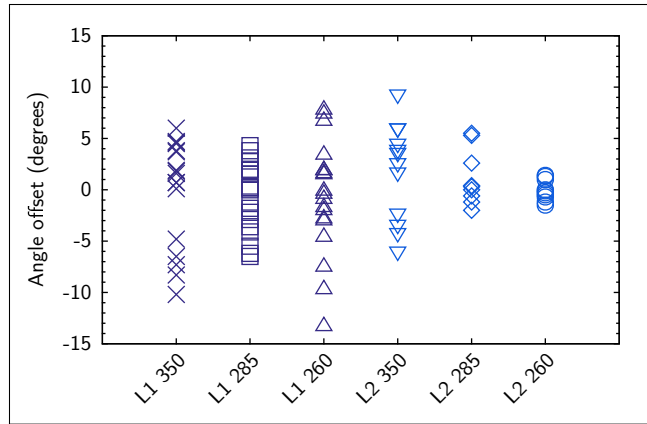

Fig. 11. Offset in the angular orientation of two laser die with respect to the trap, for different sizes of the trap. The labels L1 and L2 correspond to the die of Figs. 9 and 10, respectively. The numbers 350, 285 and 260 correspond to the size of the trap in μm.

individual measurements is $1.4\,\mu m$ for the distances and $0.4°$ for the angles.

In a previous work [16] we explored the accuracy of optoelectronic tweezers when performing small displacements in a given direction and small rotations with the same InP microlasers used in the present work. The results indicated accuracies better than $2\,\mu m$ and $2°$, with an error of $\pm 1\,\mu m$ for the measurement of the absolute travelled distance and $\pm 0.5°$ for the absolute rotation.

The positional accuracy is at the limit of what would be useful in terms of the associated coupling losses, and the angular accuracy would be good enough for components that are not

far from each other [5, 17].

Future work involves the design of a strategy to electrically contact the microlasers. An interesting possibility is to realise the contact within the optoelectronic tweezers device itself through positioning of solder beads at the edges of the microlaser and further heating. The dielectrophoretic trap could be kept on during the process to ensure the lasers do not change their position. Another possibility is to use mechanical stops such as mesas on the substrate or to bring the die into a recess on the silicon substrate. Finally, pre-deposited metal layers could also be used after moving the die on top of them. While the movement of the laser is limited to the surface of the silicon, it is possible to move them onto thin metal layers (of the order of a few hundred nanometres thick). A problem that will have to be solved is what to do with the roughly 50% of microlasers that land upside down, that is with their bottom contact face up. One possibility is to discard those and put them back into the pool for later reuse.

5. Conclusion

We have reported the accuracy of the positioning of standard Fabry-Pérot InP semiconductor laser die with optoelectronic tweezers. The results indicate that, after movement of the dielectrophoretic trap, the microlasers can be centred within the trap with a positional and angular accuracy of 2.5 ± 1.4 µm and 1.4 ± 0.4 °, respectively. This positional accuracy is at the limit of what would be acceptable for positioning in a photonic platform, but the angular accuracy would be good enough for components that are not far from each other.

The dependence of the accuracy with the size of the trap can be explained with the help of the simulations. Furthermore, comparison of the simulations using two different formalisms with the experimental observations leads us to conclude that the effective dipole moment approximation is not valid for the InP semiconductor lasers, and the Maxwell stress tensor formalism should be used instead.

The results of the accuracy reported in this work are in good agreement and complement previous results that explored the accuracy in the absolute travelled distance for small displacements and rotations. While those previous results give an idea of how accurately the position of a microlaser can be corrected when it is close to the final intended position, the results presented here give a more general estimate of how accurately the microlasers can be brought from their original position to an arbitrary final location in the device.

We believe there is room for improvement of the accuracy and the systematic misalignment with respect to the nominal centre of the trap by carefully setting up the optical path of the projected dielectrophoretic trap and by seeking ways to reduce the friction between the laser die and the a-Si:H surface.

Our results and previously published works indicate that optoelectronic tweezers are a promising technique for the micromanipulation and alignment of light sources and other optoelectronic components of a wide range of sizes (from hundreds of nanometres to hundreds of micrometres) for integration on a photonic platform in applications from communications to sensing. Indeed, previous work with smaller microdisk lasers and nanowieres, as well as current work with solder beads indicates that smaller components are easier to manipulate, possibly due to a smaller influence of the mass and much smaller contact surface and therefore reduced friction.

Acknowledgements